RSC Advances

ROYAL SOCIETY OF CHEMISTRY

www.rsc.org/advances

Journal Name

RSCPublishing

ARTICLE

Preparation of Flexible Reduced Graphene Oxide/ Poly (vinyl alcohol) Film with Superior Microwave Absorption Property

Cite this: DOI: 10.1039/x0xx00000x

Tihong Wang,[a] Yongfeng Li,[a*] Sai Geng,[a] Chen Zhou,[a] Xilai Jia,[a] Fan Yang,[a] Liqiang Zhang,[a] Xiao Ren,[b] and Haitao Yang[b*]

Received 00th January 2012,
Accepted 00th January 2012

DOI: 10.1039/x0xx00000x

www.rsc.org/

Large-area reduced graphene oxide (rGO)/poly(vinyl alcohol) (PVA) film with excellent microwave absorption property has been prepared by a simple solution processing method. Excellent interfacial interaction between GO and PVA has been realized due to the molecule-level dispersion. Characterizations of X-ray diffraction, the Fourier transform infrared (FT-IR) spectra, X-ray photoelectron spectrum and Raman spectroscopy have confirmed the reduced process of GO in the composites. The rGO/PVA film exhibits excellent microwave absorbing properties in the range of 2-18 GHz. It is expected to be a promising candidate as one of microwave absorbing materials.

Introduction

In recent days, electromagnetic (EM) wave absorbing materials have aroused great interests in civil and military fields because of EM wave pollution. In order to obtain EM wave absorbing materials with excellent EM absorption properties, the materials need to have a strong absorbing capability and meet requirement of impedance matching. It is well known that both absorbing capability and impedance matching are related to permittivity. Therefore, we can obtain composites with excellent EM absorption properties by controlling the permittivity.

Recently, graphene and its related materials are reported as the high-performance EM wave absorbing materials due to their much better intrinsic properties, such as higher conductivity, higher specific surface area and lower density, compared to traditional absorbing materials.[1-3] In addition, low cost graphene can be produced in bulk through a chemical oxidation and reduction process using graphite as the raw material. For GO, there are many oxygen-containing functional groups like hydroxyl, carbonyl groups, epoxy and carboxy on the plane. Because of these functional groups which can significantly alter van der Waals interactions among the layers of graphene, GO can disperse in various polar solvent or potentially form hydrogen bond with other materials readily.[4] The reduced graphene oxide (rGO) product can be obtained through reduction process and in which, generally speaking, hydrazine,[4-6] hydrothermal process[7-11] and thermal reduction[12, 13] are mostly used. In recent years, L-ascorbic acid was reported to reduce GO because it is friendly.[14-16]

Up to now, many researchers have studied the EM absorption property of rGO or its related materials and demonstrated that they have good EM absorption properties. Zhang *et al* have demonstrated the broadband and tunable high-performance microwave absorption (MA) property of an ultralight and highly compressible graphene foam (GF).[7] Wang *et al.* have fabricated GO/CNT-Fe_3O_4 composites by using a one-pot co-precipitation *in-situ* growth route and found that the composite took on both dielectric loss and magnetic loss.[17] Kong *et al* prepared CNT/G hybrids using *in-situ* grown method and CNT/G hybrids were dispersed into poly (dimethyl siloxane). The RC_{min} of composites can reach -55 dB; while the effective absorption bandwidth reaches 3.5 GHz in X-band when the filler loading is 5 wt.% and thickness of absorber is 2.75 mm.[18] Yu *et al* synthesised graphene/polyaniline nanorod arrays and found that the poor EM absorption properties of graphene can be significantly improved by the growth of the PANI nanorod arrays on the graphene sheets.[19] In addition, Chen utilized hydrazine to reduce GO, and epoxy composites with 15 wt% of the resulting graphene fillers exhibiting the highest electromagnetic shielding of 21 dB in the X-band.[6] Bai *et al* prepared chemically reduced GO/polyethylene oxide composites and they found that RL can up to -38.8 dB and bandwidth can up to 5.6 GHz.[16] Zhang *et al* used a simple hot-press to synthesize the RGO/CuS/PVDF composites, which exhibit high values of reflection loss and the maximum loss is 32.7 dB at 10.7 GHz when the thickness is just 2.5 mm.[20] Moreover, there are many other

[a]*State Key Laboratory of Heavy Oil Processing, China University of Petroleum, Beijing, Changping 102249, P. R. China. Phone/Fax: +86-010-89739028. E-mail: yfli@cup.edu.cn*

[b]*Beijing National Laboratory for Condensed Matter Physics, Institute of Physics, Chinese Academy of Sciences, Beijing 100190, P. R. China. E-mail: htyang@aphy.iphy.ac.cn*

composites, such as rGO/α-Fe_2O_3,[21-23] PVDF/GO,[12] rGO/Fe_3O_4,[24-27] and rGO/ZnO hollow sphere[28] are reported for EM absorbing.

Despite reported composites have good EM wave absorption properties in some cases, their drawbacks, such as high density, poor stability, and large loading content, have severely hindered their practical applications. Moreover, most researchers use paraffin as matrix when they do such EM absorption measurement. This will restrict the practical application of materials immensely. Meanwhile, due to the existence of strong van der Waals interaction and the out-of-plane π bond between the individual graphene nanosheet, it is difficult to avoid irreversible agglomeration or even restacking for graphene and its related materials. As we all know, its agglomeration or restacking will hamper the applications of graphene in various fields.

Here, we prepared large-area rGO/PVA EM wave absorbing film using a simple solution processing method. GO is dispersed in PVA at the molecular level and there are strong interfacial interactions between rGO and matrix PVA. The as-prepared composites show excellent EM wave absorption properties because of charge transfer, interfacial polarization, favourable impedance matching and so on.

Experimental

Materials

Graphite powder (200 mesh, Alfa Aesar, Johnson Matthey Company). $KMnO_4$, $K_2S_2O_8$, P_2O_5, H_2O_2 (Beijing Chemical Works), poly(vinyl alcohol) 1788 (Sinopec Shanghai petrochemical co., LTD). All chemicals were analytical grade and used directly without further purification.

Preparation of GO/PVA film

Graphene oxide (GO) was synthesized from natural graphite powder by a modified Hummers method.[29,30] Exfoliation was carried out by ultrasonicating the GO dispersion into deionized (DI) water under ambient conditions for 1 h. For the preparation of rGO/PVA film, PVA (5 g) was dissolved in distilled water (100 mL) at 50 °C and the solution was subsequently cooled to room temperature.[31] Meanwhile, 50 mL of a 1 mg/mL GO suspension was ultrasonicated for 0.5 h. Then, the GO suspension was gradually added to the PVA solution and sonicated for another 30 min. After that, the homogeneous GO/PVA solution was transferred to flask. Finally, L-ascorbic acid (500 mg) was added into mixture solution and stirred at 50 °C for 24 h. When the reaction ended, the colour of the mixture solution turned from yellow to black. The film can be obtained when the solution was dried under vacuum at 60 °C until its weight kept constant.

Characterization

X-ray diffraction (XRD) patterns were carried out on a Bruker D8 Advance X-ray diffractometer using Cu Kα (λ=1.54Å) radiation. The Fourier transform infrared (FT-IR) spectra were collected with a Magna-IR 560 E.S.P spectrometer. Raman spectra were recorded on a Renishaw inVia confocal Raman microscope system using green (532 nm) laser excitation. The X-ray photoelectron spectrum (XPS) was conducted on a Thermo Fisher K-Alpha spectrometer.

EM absorption measurement

The toroidal-shape (Φ_{out} = 7.00 mm and Φ_{in} = 3.04 mm) of composites came out from a mold for EM absorption measurement. The complex permittivity and permeability values were measured in the 2-18 GHz range with the coaxial line method by an Agilent N5224A vector network analyzer.

Results and discussion

Fig. 1a shows the picture of the film containing 0.9 wt% GO, which is smooth, uniform. Meanwhile, the thickness of the film can be controlled by the amount of the solution used for film. What is more, it can be cut into various shapes and different sizes by a scissor and it can be bended at any angle, as shown in Figs. 1b and 1c. This is convenient and favourable for practical application. Fig. 1d shows the patterns of GO, PVA and rGO/PVA films. We can see that the characteristic XRD diffraction peak of pure GO is appeared at 2θ=10.3°, implying that the distance between layers is about 0.84 nm. We can also see that the characteristic XRD diffraction peak of PVA is found at about 2θ=19.5°. Interestingly, the XRD pattern of rGO/PVA film has only one peak at about 2θ=19.5°, indicating that GO has been uniformly dispersed in PVA matrix and rGO cannot restack in the reduction process. Meanwhile, the crystalline structure of PVA was slightly affected by the incorporation of rGO.

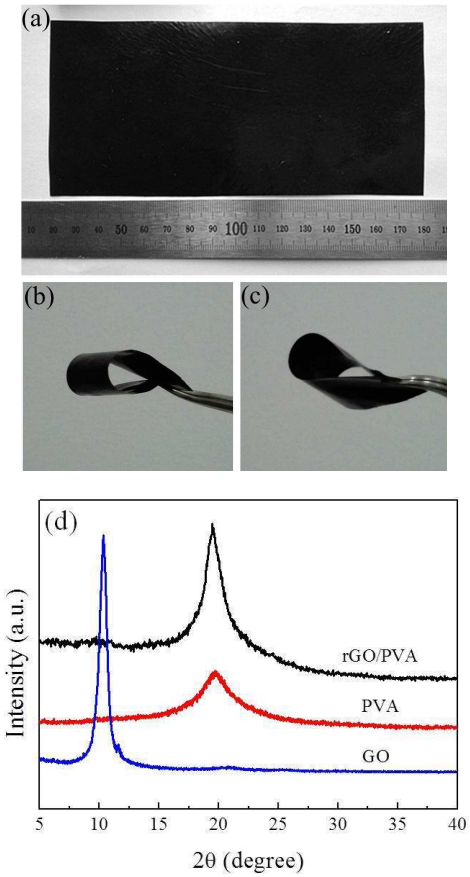

Fig. 1 The picture of rGO/PVA film (a, b and c) and XRD patterns of GO, pure PVA and rGO/PVA (d).

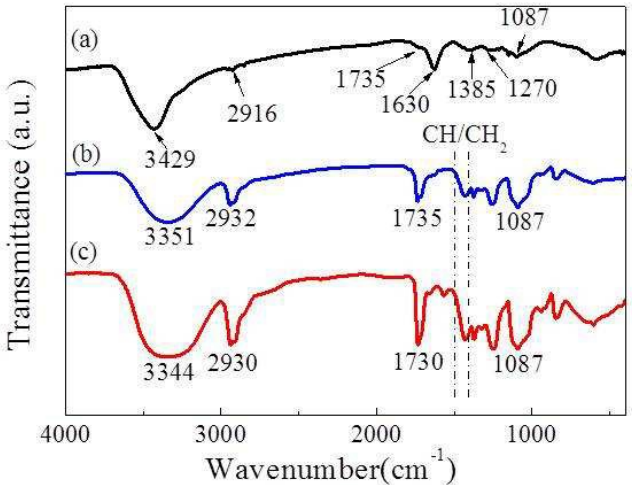

Fig. 2 FT-IR spectra of GO (a), pure PVA (b) and rGO/PVA film (c).

Fig. 2 shows the FT-IR spectra of GO, the PVA film and the rGO/PVA film. In the spectrum of GO, we observe a strong and broad absorption at 3429 cm^{-1} due to O-H stretching vibration of carboxyl groups and the absorbed water. The peaks at 1385 and 1270 cm^{-1} correspond to the skeletal vibrations of C-OH and C-O-C. The characteristic peak for C=O stretching vibration appears at 1735 cm^{-1}. The peak at 1630 cm^{-1} corresponds to C=C skeletal stretching vibration. From the spectra of PVA and rGO/PVA film, we can see that there is absorption peak between 3000 cm^{-1} and 3500 cm^{-1}, which is the O-H stretching, indicating the existence of strong intermolecular and intramolecular hydrogen bonding.[32] For pure PVA, the O-H vibration peak occurs at 3351 cm^{-1}. This absorption peak is shifted to 3344 cm^{-1}, a lower wavenumber with the addition of rGO. Meanwhile, the stretching vibration of C=O shifts to1730 cm^{-1}, appearing with higher intensity in the rGO/PVA spectrum, indicating that hydrogen bond between C=O and OH has been established. These phenomena indicate the existence of hydrogen bonding between the hydroxyl group in PVA and the remaining oxygen-containing functional groups in rGO.[33, 34] Moreover, in the FT-IR spectra of GO and PVA, a stretching vibration band at 2800-3000 cm^{-1} belonging to C-H_2 is observed. When rGO was added into PVA, the intensity of stretching vibration band at 2800-3000 cm^{-1} becomes stronger. The films also show a deformation vibration band at 1300-1500 cm^{-1} (CH/CH_2 deformation vibrations). The above results prove the strong interfacial interaction between rGO and PVA.

The XPS measurements also proved the reduction process. As shown in Fig. 3a, the bands in the wide scan of GO and rGO/PVA are C1s and O1s. Fig. 3b shows the C1s spectra acquired from GO. In the GO sample, three different peaks centered at 284.6, 286.4, 288 eV, corresponding to C=C/C-C in aromatic rings, C-O (epoxy and alkoxy) and C=O groups are observed. GO possesses high hetercarbon components like the functional groups of C-O and C=O.[35, 36] The above result suggests that GO contains large numbers of functional groups on its surface. Fig. 3c shows the C1s spectra from rGO/PVA, although there are heterocarbon on rGO, the absorbance intensity decreases sharply. The results indicate that the graphitic structure remarkably restored through reduction process.

Fig. 4 shows the Raman spectra of pure PVA, GO and rGO/PVA. The pure PVA has no Raman signal in the range of 1000–2000 cm^{-1}. By comparison, the characteristic peaks at 1345 and 1592 cm^{-1} appear, corresponding to D band and G band for GO. For rGO/PVA, D and G bands are located at 1307 and 1590 cm^{-1}, respectively. The intensity ratio of the D band to the G band for GO and rGO/PVA is 1.1 and 2.1. The change of D/G ratio suggests the generation of a larger number of sp^2 carbon domains with a smaller average size in rGO/PVA.[37] We also found that the location of D and G band shifted to lower wavenumber. The reason of location of D and G shifted from high wavenumber to low wavenumber maybe is the recovery of the hexagonal network of carbon atom.

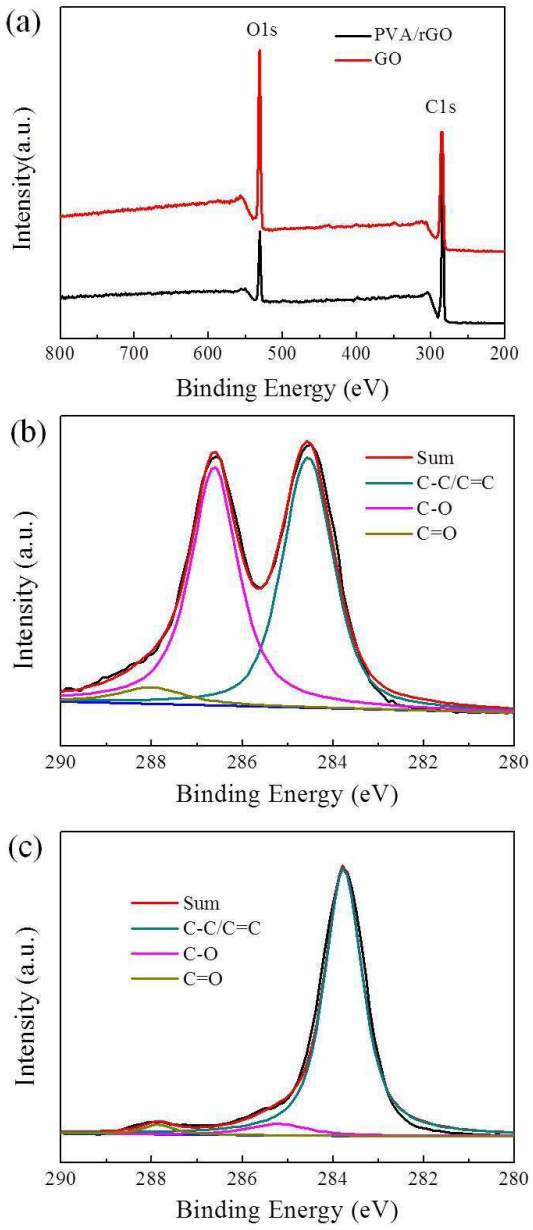

Fig. 3 XPS spectra of GO and rGO/PVA film (a) and C1s for GO (b) and rGO/PVA film (c).

EM absorption properties of rGO/PVA film

Fig. 5a and b show the frequency dependence of the real part (ε′) and imaginary part (ε″) of relative complex permittivity ($\varepsilon_r = \varepsilon' - j\varepsilon''$) for the rGO/PVA film with 0, 0.9 wt% and 3.2 wt% rGO. According to Fig. 5a, the values of ε′ decrease from 3.6 to 2.8, 12.75 to 5.84 and 36.8 to 16.8, with increasing frequency increases in the range of 2-18 GHz, respectively. In addition, the values of ε′ significantly increase with the increase in mass percentage of rGO in the composites.

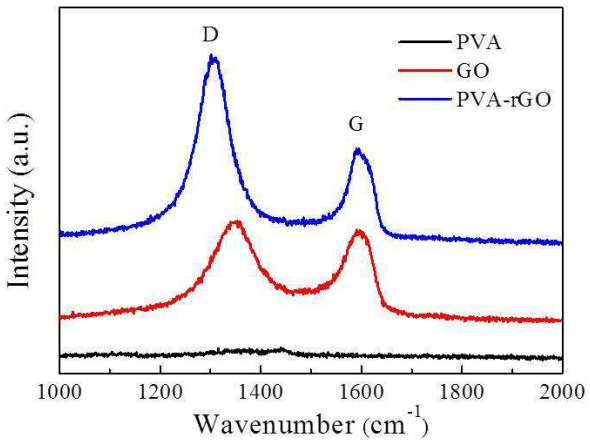

Fig. 4 Raman spectra of pure PVA, GO and rGO/PVA film.

The reason for this phenomenon is that the increasing amounts of rGO increase the dipolar polarization and electrical conductivity. Similarly, as shown in Fig. 5b, the values of ε″ are in the range of 0.18-0.38, 2.6-4 and 4.8-12.6, corresponding to pure PVA, 0.9 wt% rGO/PVA and 3.2 wt% rGO/PVA, respectively. For pure PVA, the ε″ values are very close to zero, indicating very poor dielectric loss of pure PVA. We can also see that the values of ε″ prove nonlinear behaviour, but it also increases with the increase in mass percentage of rGO in the range of 2-18 GHz. Generally, we use the dielectric loss tangent ($\tan \delta_E = \varepsilon''/\varepsilon'$) to evaluate the performance of EM wave absorption. Fig. 5c shows the tangent of pure PVA, 0.9 wt% rGO/PVA and 3.2 wt% rGO/PVA. Pure PVA shows quite low dielectric loss tangent in the whole frequency range due to its small ε″ values. We can see that the values of tangent also exhibit nonlinear behaviour. For 0.9 wt% rGO/PVA and 3.2 wt% rGO/PVA, they have strong dielectric loss. This result demonstrates that the good EM wave absorption property could be caused by dielectric loss.

To evaluate the EM absorption properties of composites, its reflection loss (RL) are calculated according to the transmit line theory:

$$Z_{in} = \sqrt{\frac{\mu_r}{\varepsilon_r}} \tanh[j(\frac{2\pi fd}{c})\sqrt{\mu_r \varepsilon_r}] \quad (1)$$

$$RL = 20\log\left|\frac{Z_{in}-1}{Z_{in}+1}\right| \quad (2)$$

where Z_{in} is the normalized input impedance of the microwave absorption layer, ε_r and μ_r are the relative permittivity and permeability of the materials, j is the microwave frequency, d is the thickness of the absorber and c is the velocity of light in free space.

Fig. 6 shows the calculated theoretical RL of pure PVA, 0.9 wt% rGO/PVA and 3.2 wt% rGO/PVA film with different thickness in the range of 2-18 GHz. As shown in Fig. 6a, the pure PVA has very weak EM absorption property at every sample thickness except for nearly 18 GHz. In contrast, as shown in Fig. 6b and c we can find that when GO was added into PVA, the values of RL was dramatically improved. Meanwhile, for rGO/PVA EM absorption film, it is found that the thickness of the sample is one of major factors, which affects not only the intensity of the reflection loss peak but also the position of the frequency at the reflection minimum. The detail is that the

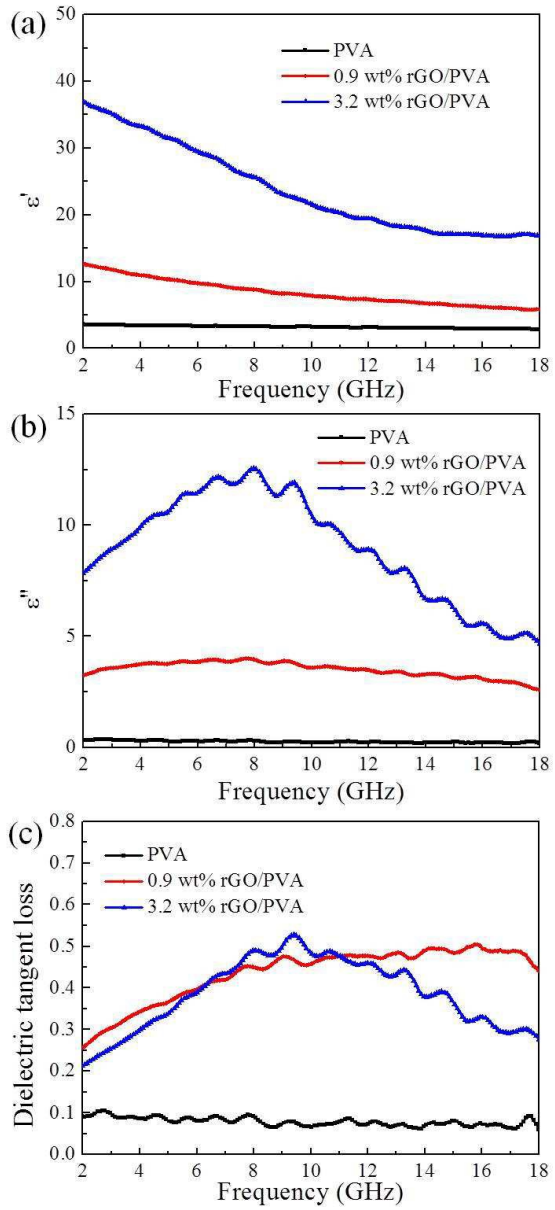

Fig. 5 Frequency dependence of real part (a) and imaginary part (b) of relative complex permittivity, dielectric loss tangent (c) of pure PVA, 1 wt% rGO /PVA and 1 wt% rGO /PVA film.

minimum RL increases and shifts towards a lower frequency with increasing thickness. The peak shift is attributed to the phenomena of

quarter-wavelength attenuation, in which the absorption meets the phase match conditions.[38] The minimum RL is -36.4 dB when the mass percentage of GO is 0.9 wt% and the thickness is 5 mm at 4.5 GHz. In addition, when the thickness of film is 2 mm, the bandwidths of RL values below -10 dB (90% of EM wave absorption) can exceed 7.7 GHz. Compared with previous reports such as ternary $BaTiO_3$/MWNT/PBO,[39] CMK-3/PMMA composites,[40] Fe_3O_4/Al_2O_3/CNCs,[3] rGO/α-Fe_2O_3,[21-23] PVDF/GO,[12] RGO/CuS/PVDF,[20] rGO/Fe_3O_4,[24-26] rGO/ZnO hollow sphere[28] and C-RG/PEO,[16] as-prepared rGO/PVA films perform a better EM wave absorption.

Fig. 6c shows the RL of rGO/PVA film with GO loading of 3.2 wt%. We can see that its EM wave absorption property is weaker than that of 0.9 wt %

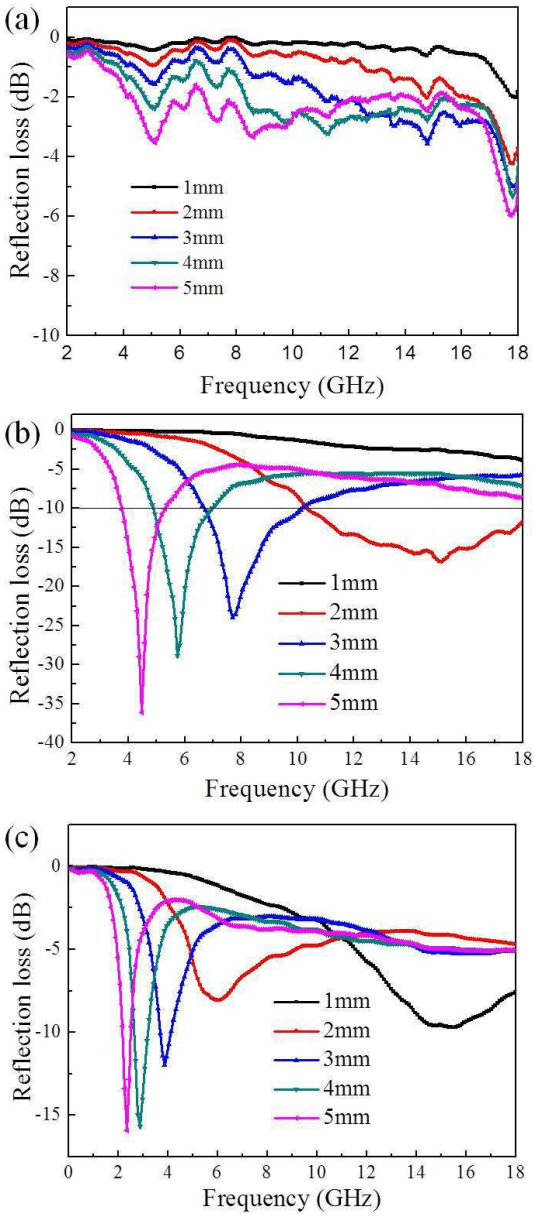

Fig. 6 The reflection loss of pure PVA film (a), 0.9 wt% rGO/PVA film (b) and 3.2 wt% rGO/PVA film (c) with different thickness from 1 to 5 mm.

rGO/PVA. The reason for above phenomenon is possible duo to the too high ε′. Interestingly, when thickness thickens, the good EM wave absorption can be shown in the range of 2-4 GHz. It is mainly due to the increases of interface between PVA and rGO and electrical conductivity is caused by more rGO existing in rGO/PVA film. The more interfaces, the more interfacial polarization, which will be more easily induced at lower frequency.

The reason why rGO/PVA film shows superior EM absorption property is that it has a strong absorbing capability and it can greatly meet the requirements of impedance matching, as schematically shown in Fig. 7. Firstly, rGO is absorber material and we can realize dispersion at molecule-level in PVA because of hydrogen bond which exists between rGO and PVA. For rGO, there still are defects and residual oxygen functional groups, these functional groups and defects can act as polarized centers and enhance orientation polarization. Besides, carbon atom and oxygen arom have different abilities to catch electrons, this can result in electronic dipole polarization. There are electron polarization, ion polarization and molecular polarization. More importantly, there exist many interfaces between rGO and PVA trigging interfacial polarization. Furthermore, the accumulation of free charges gives rise to the strong interfacial polarization and leads to the increase of EM wave absorption. The charge transfer occurring at the interface can enhance the intensity of the Debye dipolar relaxation, which can increase EM wave absorption. What's more, rGO can form local conductive network, which will establish eddy under EM wave. So, EM wave can convert into heat easily. In addition, rGO is so small, highly structured and porous and it can scatter EM wave. Besides, we can regard PVA as dielectric material, which possesses a wide range of wave-transparent property change. The substance of wave-transparent is providing channels for transmission of EM wave. As for EM wave absorbing composites, dielectric material plays a leading role in adjusting input impedance. Only material has good wave-transparent, can it provide a guarantee of broadband for EM wave absorbing composites. At the same time, it can create conditions for absorber material. As discussed above, with the synergistic effect of the rGO and PVA, the as-prepared rGO/PVA films exhibit superior EM wave absorption properties.

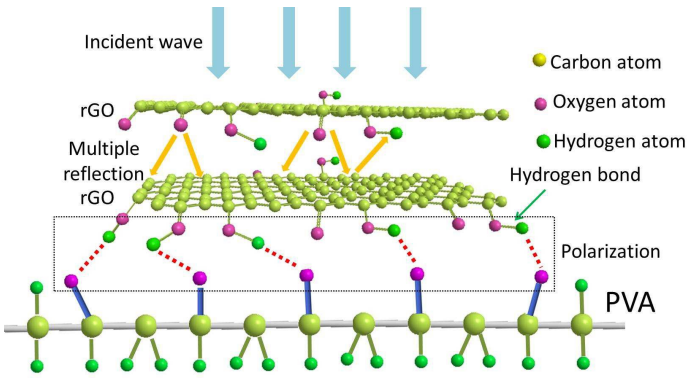

Fig. 7 The possible microwave absorbing mechanism of rGO/PVA film.

Conclusions

In summary, a simple solution processing method is employed for preparation of rGO/PVA film, which is free-standing, robust and flexible. In this process, GO was *in-situ* reduced by L-AA in PVA solution to form rGO/PVA uniformly. There exist a lot of hydrogen bonds between rGO and PVA. So, rGO can be dispersed in PVA at molecule-level instead of agglomeration or restack. The dielectric constant of the composites increases with the introduction of rGO. For 0.9 wt% rGO/PVA film, the minimum RL is -36.4 dB when the thickness is 5 mm at 4.5 GHz. In addition, when the thickness of film is 2 mm, the bandwidths of RL values below -10 dB (90% of EM wave absorption) can exceed 7.7 GHz. The main microwave absorbing mechanism of rGO/PVA composite is dielectric loss caused by relaxation process that includes interfacial polarization, the Debye dipolar relaxation, electronic dipole polarization and orientation polarization. It can be believed that the rGO/PVA film can be used as effective material for microwave absorption.

Acknowledgements

We gratefully thank for the National Natural Science Foundation of China (No. 21322609 and 21202203), the Science Foundation Research Funds Provided to New Recruitments of China University of Petroleum, Beijing (No. 2462014QZDX01, YJRC-2013-31), the National Basic Research Program of China (No. 2012CB933102), and Thousand Talents Program.

Notes and references

1. Z. Chen, W. Ren, L. Gao, B. Liu, S. Pei and H.-M. Cheng, *Nat. Mater.*, 2011, **10**, 424-428.
2. Z. Chen, C. Xu, C. Ma, W. Ren and H.-M. Cheng, *Adv. Mater.*, 2013, **25**, 1296-1300.
3. G. Wang, Z. Gao, S. Tang, C. Chen, F. Duan, S. Zhao, S. Lin, Y. Feng, L. Zhou and Y. Qin, *ACS Nano*, 2012, **6**, 11009-11017.
4. S. Stankovich, D. A. Dikin, G. H. B. Dommett, K. M. Kohlhaas, E. J. Zimney, E. A. Stach, R. D. Piner, S. T. Nguyen and R. S. Ruoff, *Nature*, 2006, **442**, 282-286.
5. D. Li, M. B. Muller, S. Gilje, R. B. Kaner and G. G. Wallace, *Nat. Nano.*, 2008, **3**, 101-105.
6. J. Liang, Y. Wang, Y. Huang, Y. Ma, Z. Liu, J. Cai, C. Zhang, H. Gao and Y. Chen, *Carbon*, 2009, **47**, 922-925.
7. Y. Zhang, Y. Huang, T. Zhang, H. Chang, P. Xiao, H. Chen, Z. Huang and Y. Chen, *Adv. Mater.*, 2015, **27**, 2049-2053.
8. Z.-S. Wu, S. Yang, Y. Sun, K. Parvez, X. Feng and K. Müllen, *J. Am. Chem. Soc.*, 2012, **134**, 9082-9085.
9. J. Kim, W.-H. Khoh, B.-H. Wee and J.-D. Hong, *RSC Adv.*, 2015, **5**, 9904-9911.
10. L. Xiao, D. Wu, S. Han, Y. Huang, S. Li, M. He, F. Zhang and X. Feng, *ACS Appl. Mater. Interfaces*, 2013, **5**, 3764-3769.
11. C. Hu, Z. Mou, G. Lu, N. Chen, Z. Dong, M. Hu and L. Qu, *Phys. Chem. Chem. Phys.*, 2013, **15**, 13038-13043.
12. X.-J. Zhang, G.-S. Wang, W.-Q. Cao, Y.-Z. Wei, M.-S. Cao and L. Guo, *RSC Adv.*, 2014, **4**, 19594-19601.
13. R. Rozada, J. I. Paredes, M. J. Lopez, S. Villar-Rodil, I. Cabria, J. A. Alonso, A. Martinez-Alonso and J. M. D. Tascon, *Nanoscale*, 2015, **7**, 2374-2390.
14. J. Gao, F. Liu, Y. Liu, N. Ma, Z. Wang and X. Zhang, *Chem. Mater.*, 2010, **22**, 2213-2218.
15. J. Zhang, H. Yang, G. Shen, P. Cheng, J. Zhang and S. Guo, *Chem. Commun.*, 2010, **46**, 1112-1114.
16. X. Bai, Y. Zhai and Y. Zhang, *J. Phys. Chem. C*, 2011, **115**, 11673-11677.
17. L. Wang, X. Jia, Y. Li, F. Yang, L. Zhang, L. Liu, X. Ren and H. Yang, *J. Mater. Chem. A*, 2014, **2**, 14940-14946.
18. L. Kong, X. Yin, X. Yuan, Y. Zhang, X. Liu, L. Cheng and L. Zhang, *Carbon*, 2014, **73**, 185-193.
19. H. Yu, T. Wang, B. Wen, M. Lu, Z. Xu, C. Zhu, Y. Chen, X. Xue, C. Sun and M. Cao, *J. Mater. Chem.*, 2012, **22**, 21679-21685.
20. X.-J. Zhang, G.-S. Wang, Y.-Z. Wei, L. Guo and M.-S. Cao, *J. Mater. Chem. A*, 2013, **1**, 12115-12122.
21. T. Wang, Y. Li, L. Wang, C. Liu, S. Geng, X. Jia, F. Yang, L. Zhang, L. Liu, B. You, X. Ren and H. Yang, *RSC Adv.*, 2015, **5**, 60114-60120.
22. D. Chen, G.-S. Wang, S. He, J. Liu, L. Guo and M.-S. Cao, *J. Mater. Chem. A*, 2013, **1**, 5996-6003.
23. H. Zhang, A. Xie, C. Wang, H. Wang, Y. Shen and X. Tian, *J. Mater. Chem. A*, 2013, **1**, 8547-8552.
24. E. Ma, J. Li, N. Zhao, E. Liu, C. He and C. Shi, *Mater. Lett.*, 2013, **91**, 209-212.
25. H. Zhang, C. Zhu, Y. Chen and H. Gao, *ChemPhysChem*, 2014, **15**, 2261-2266.
26. Y. Zhan, F. Meng, Y. Lei, R. Zhao, J. Zhong and X. Liu, *Mater. Lett.*, 2011, **65**, 1737-1740.
27. H.-L. Xu, H. Bi and R.-B. Yang, *J. Appl. Phys.*, 2012, **111**, 07A522.
28. M. Han, X. Yin, L. Kong, M. Li, W. Duan, L. Zhang and L. Cheng, *J. Mater. Chem. A*, 2014, **2**, 16403-16409.
29. W. S. Hummers and R. E. Offeman, *J. Am. Chem. Soc.*, 1958, **80**, 1339-1339.
30. Y. Liang, D. Wu, X. Feng and K. Müllen, *Adv. Mater.*, 2009, **21**, 1679-1683.
31. J. Liang, Y. Huang, L. Zhang, Y. Wang, Y. Ma, T. Guo and Y. Chen, *Adv. Funct. Mater.*, 2009, **19**, 2297-2302.
32. S. Gahlot, P. P. Sharma, V. Kulshrestha and P. K. Jha, *ACS Appl. Mater. Interfaces*, 2014, **6**, 5595-5601.
33. M. Cano, U. Khan, T. Sainsbury, A. O'Neill, Z. Wang, I. T. McGovern, W. K. Maser, A. M. Benito and J. N. Coleman, *Carbon*, 2013, **52**, 363-371.
34. H. Beydaghi, M. Javanbakht and E. Kowsari, *Ind. Eng. Chem. Res.*, 2014, **53**, 16621-16632.
35. H. Ha, K. Shanmuganathan and C. J. Ellison, *ACS Appl. Mater. Interfaces*, 2015, **7**, 6220-6229.
36. D. R. Dreyer, S. Park, C. W. Bielawski and R. S. Ruoff, *Chem. Soc. Rev.*, 2010, **39**, 228-240.
37. V. C. Tung, M. J. Allen, Y. Yang and R. B. Kaner, *Nat. Nano.*, 2009, **4**, 25-29.
38. L. Kong, X. Yin, Y. Zhang, X. Yuan, Q. Li, F. Ye, L. Cheng and L. Zhang, *J. Phys. Chem. C*, 2013, **117**, 19701-19711.
39. J. Wei, S. Zhang, X. Liu, J. Qian, J. Hua, X. Li and Q. Zhuang, *J. Mater. Chem. A*, 2015, **3**, 8205-8214.
40. H. Zhou, J. Wang, J. Zhuang and Q. Liu, *Nanoscale*, 2013, **5**, 12502-12511.

